JPE 15-6-4

http://dx.doi.org/10.6113/JPE.2015.15.6.1446
ISSN(Print): 1598-2092 / ISSN(Online): 2093-4718

Resonant Tank Design Considerations and Implementation of a LLC Resonant Converter with a Wide Battery Voltage Range

Wenjin Sun*, Hongfei Wu*, Haibing Hu†, and Yan Xing*

*,†Jiangsu Key Laboratory of Renewable Energy Generation and Power Conversion,
College of Automation Engineering, Nanjing University of Aeronautics and Astronautics, Nanjing, China

Abstract

This paper illustrates resonant tank design considerations and the implementation of a LLC resonant converter with a wide battery voltage range based on the fundamental harmonic approximation (FHA) analysis. Unlike the conventional design at zero load, the parameter K (the ratio of the transformer magnetizing inductor L_m to the resonant inductor L_r) of the LLC converter in this paper is designed with two charging points, (V_{o_min}, I_{o_max1}) and (V_{o_max}, I_{o_max2}), according to the battery charging strategy. A 2.9kW prototype with an output voltage range of 36V to 72V dc is built to verify the design. It achieves a peak efficiency of 96%.

Key words: Charger, FHA, LLC, Resonant converter

I. INTRODUCTION

Since electric vehicles have developed so quickly, high capacity battery packs have been widely used. However, this highly demands high efficiency, low cost and compact smart chargers. Among the currently available charging solutions, the most common charger architecture consists of an ac-dc converter with power factor correction and an isolated dc-dc converter for galvanic isolation, as shown in Fig. 1 [1]-[3].

In Fig. 1, zero-voltage switching (ZVS) topologies are preferable for the isolated second stage to enhance efficiency. In particular, the multi resonance LLC topology has several advantages over other ZVS topologies. These advantages include: (a) the ability to operate with ZVS over a wide load range; (b) no diode reverse recovery losses through soft commutation; (c) low voltage stress of the output diodes; (d) only a capacitor as an output filter compared with the conventional LC filters; and (e) few EMI issues [3]. However, the LLC topology is difficult to analyze and to achieve an optimal design due to its multi resonance.

Manuscript received Sep. 13, 2014; accepted May 21, 2015
Recommended for publication by Associate Editor Joung-Hu Park.
†Corresponding Author: huhaibing@nuaa.edu.cn
Tel: +86-025-84890393, Nanjing Univ. of Aeronautics and Astronautics
*Jiangsu Key Laboratory of Renewable Energy Generation and Power Conversion, College of Automation Engineering, Nanjing University of Aeronautics and Astronautics, China

To simplify the analysis of the characteristics of LLC converters, the fundamental harmonic approximation (FHA) has been developed, where the voltages and currents are assumed to be sinusoidal waveforms, thereby permitting the traditional AC circuit analysis to be employed. As a result, the approximated DC gain in mathematical expressions can be easily derived. Some frequency-domain analysis methods take high-order elements into account to improve the accuracy of the FHA, such as the extended fundamental frequency analysis and Fourier series expansion [4], [5]. However, these become cumbersome in practical use. Other approaches like the state-plane or time-domain analysis are based on the converter's exact model to provide precise description of the circuit behavior. However, they are usually not very easy to interpret and can be difficult to use [6], [7]. Although the accuracy of the FHA will be degraded when the switching frequency deviates far from the resonant point, it still can meet the requirements of engineering. Moreover, it is simpler and more straightforward to calculate the dc gain and design the LLC converter. Therefore, it is adopted here to analyze wide output range applications.

Despite the aforementioned advantages, it is challenging to achieve an overall high efficiency over a wide battery voltage range [3]. In this paper, by combining the features of the LLC converter and the characteristics of the battery charging profile, an optimal design procedure is proposed to achieve

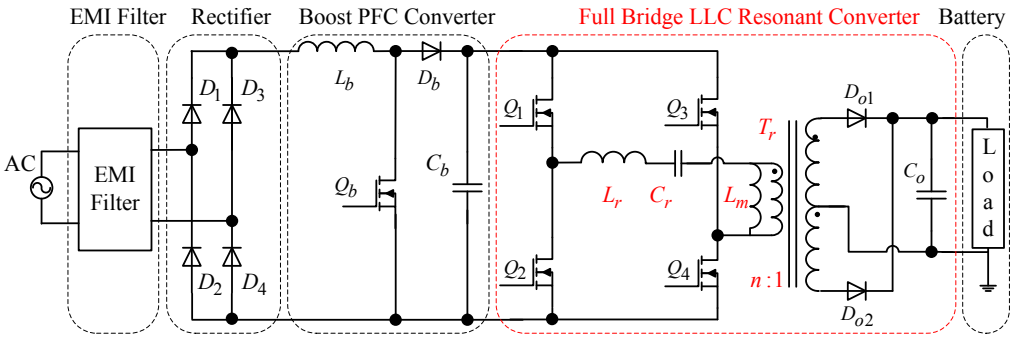

Fig. 1. Typical battery charging power architecture.

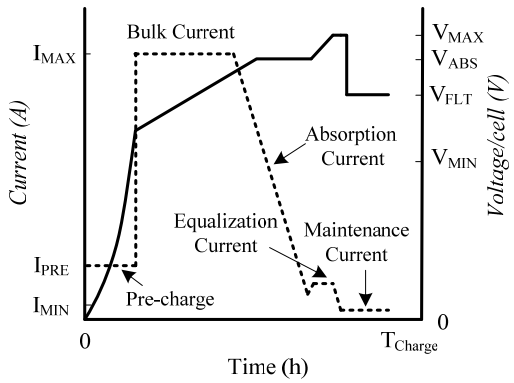

Fig. 2. Simplified lead-acid battery charging profile.

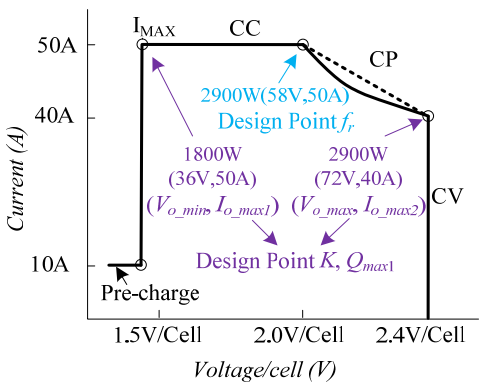

Fig. 3. Desired lead-acid battery V-I plane on a 2900 W charger.

an overall high efficiency.

Fig. 2 shows a simplified battery charging profile with five distinct operating modes: Pre-charge (Activate), Bulk, Absorption, Equalization, and Maintenance [2]. In the Pre-charge mode, the charger outputs a small current to activate the batteries. This current is about 20% of I_{MAX}. In the Bulk mode, the charger charges the batteries with a constant current I_{MAX}. It charges the batteries with a constant voltage V_{ABS} in the Absorption mode. When the current decreases to a preset value I_{MIN}, the charger enters the Equalization mode with an overvoltage to equalize the cell voltages. After the batteries are fully charged, the charger only outputs a small current to offset the internal soft discharge in the Maintenance mode.

As shown in Fig. 3, the outer range of the lead acid battery V-I plane is constrained by the pre-charge, constant current (CC), constant power (CP), and constant voltage (CV) [2]. This indicates that the voltage range of a single lead-acid battery cell is generally 1.5 V~2.4 V, with a nominal voltage of 2.0 V at the maximum output current. Then it has significantly different design requirements for the resonant tank parameters when compared with those featuring a constant output voltage. The proposed resonant tank design procedure is based on the V-I plane in Fig. 3. It decides the design constraints for the full-bridge LLC converter, especially the resonant tank parameters K (the ratio of the transformer magnetizing inductor L_m to the resonant inductor L_r), and Q_{max1} (the quality factor of the resonant tank at the minimum input voltage and the full load), which are vital in the LLC design.

As indicated in Fig. 2 and Fig. 3, a small output current is required to activate the batteries in the pre-charge mode. This lasts for a short time during the whole charging process, such as 10min. Moreover, its output power, e.g. 36 V*10 A = 360 W, is much less than the nominal power 2900 W, and the increased heat dissipation can be easily handled. However, if the pre-charge mode is considered with the resonant tank design under the PFM control, the LLC converter has a wider output range, resulting in a smaller ratio K and L_m for the same frequency range. In addition, it will increase the primary conduction and turn-off losses, and deteriorate the efficiency in normal operation [8]-[10]. Therefore, the PFM&PWM control is adopted here [11], [12]. Furthermore, the charger will run into the PWM control with a small current and a low voltage output in the pre-charge mode, such as 10 A and 1.5 V/cell. The following sections will focus on the design of the LLC resonant tank parameters with a large output power under the PFM control.

II. Resonant Tank Design Procedure

Because of its advantages over other ZVS topologies, the LLC topology has been used in many applications, such as adapters, induction heating, and fuel cells [13]-[15]. However, there are two major issues with the existing LLC design used

in industry based on the FHA analysis: 1) the output voltage is considered constant (e.g. typical for telecom applications), which is not a valid assumption in battery charging, and 2) the ratio K of L_m to L_r is designed with a minimum normalized output voltage gain M_{min} at zero load as Eq. (1) [9], which is not applicable to battery charging. Then, designing the resonant tank needs different steps for a battery charger. In the following work, the ratio K is designed with the two charging points (V_{o_min}, I_{o_max1}) and (V_{o_max}, I_{o_max2}) in Fig. 3. This is different from the design at zero load.

$$K = \frac{nM_{min}}{1-nM_{min}}(1-\frac{f_r^2}{f_{max}^2}) \quad (1)$$

Where, $M_{min} = nV_{o\_min}/V_{in\_max}$ with the transformer turn ratio n, and f_r and f_{max} are the resonant frequency and maximum switching frequency.

Based on the FHA analysis, the nonlinear circuit of the full bridge LLC resonant converter in Fig. 1 can be transformed into the linear circuit in Fig. 4, where the ac resonant tank is excited by an effective sinusoidal input source that drives an effective resistive load R_e as (2) [9]. This transformation allows for the use of traditional AC circuit analysis methods to study the circuit, and the normalized output gains of the LLC converter could be derived as (3) [9]. Fig. 5 illustrates the family of its typical characteristics.

$$R_e = \frac{8V_o}{\pi^2 I_o} \quad (2)$$

$$M(K,X,Q) = \frac{1}{\sqrt{[1+\frac{1}{K}(1-\frac{1}{X^2})]^2 + Q^2(X-\frac{1}{X})^2}} \quad (3)$$

Where, X is the normalized switching frequency f_s/f_r. Q is the resonant tank quality factor for different loads. Z_o is the characteristic impedance of the LLC resonant tank.

$$Q = Z_o/(n^2R_e) \quad (4)$$

$$Z_o = \sqrt{L_r/C_r} \quad (5)$$

For the LLC converter, as the switching frequency is varied closer to f_r, the impedance of the resonant tank becomes smaller. This can reduce the circulating energy in the resonant tank and the conduction losses of the LLC converter [3]. In addition, the maximum efficiency can be achieved at $f_s = f_r$. Thus, the charger is designed to deliver the maximum output power at the unity gain point ($f_s = f_r$), which is marked as "Design Point f_r" in Fig. 3. Furthermore, it is appropriate to operate the converter in Region 1 and Region 2 to maintain the primary switches' ZVS operation for a wide DC gain range [9].

In order to avoid the primary switches working in the ZCS turn-off condition at (V_{o_max}, I_{o_max2}) in Fig. 3, Q_{max1} at this charging point can be designed at the blue dotted boundary between ZVS Region 2 and ZCS Region 3 in Fig. 5. In addition, the imaginary part of the resonant tank input impedance $Z_{in}(j\omega)$ in Fig. 4 is zero here. Then, Q_{max1} has a relation with the inductor ratio K as (7) [9].

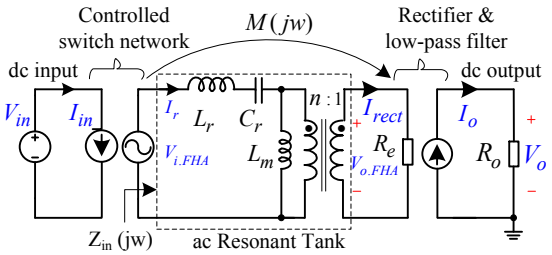

Fig. 4. Two port model for LLC resonant converter based on FHA.

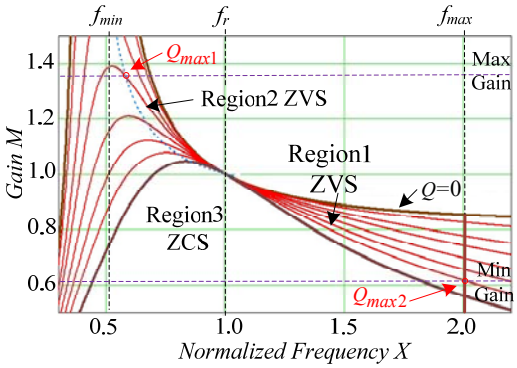

Fig. 5. Typical dc gain characteristics of the LLC converter.

$$Z_{in}(j\omega) = j\omega L_r + \frac{1}{j\omega C_r} + \frac{j\omega L_m \cdot n^2 R_e}{j\omega L_m + n^2 R_e} \quad (6)$$

$$Q_{max1} = \frac{1}{KM_{max}}\sqrt{\frac{M_{max}^2}{M_{max}^2-1}+K} \quad (7)$$

Where, $M_{max}=nV_{o\_max}/V_{in\_min}$.

If the maximum normalized switching frequency $X_{max}= f_{max}/f_r$ at (V_{o_min}, I_{o_max1}) is fixed, then its quality factor Q_{max2} can be derived from (3) as:

$$Q_{max2} = \frac{1}{X_{max}-1/X_{max}}\sqrt{\frac{1}{M_{min}^2}-[1+\frac{1}{K}(1-\frac{1}{X_{max}^2})]^2} \quad (8)$$

As determined by the resonant tank parameters, Z_o is same at the two charging points (V_{o_min}, I_{o_max1}) and (V_{o_max}, I_{o_max2}).

$$Z_o = n^2Q_{max1}R_{e\_max} = n^2Q_{max2}R_{e\_min} \quad (9)$$

$$R_{e\_max} = \frac{8V_{o\_max}}{\pi^2 I_{o\_max2}} \quad (10)$$

$$R_{e\_min} = \frac{8V_{o\_min}}{\pi^2 I_{o\_max1}} \quad (11)$$

Then, the maximum ratio K of L_m to L_r can be obtained as (12) with (7) ~ (11).

$$K = \frac{-B+\sqrt{B^2-4AC}}{2A} \quad (12)$$

Where:

$$A = \frac{1-M_{min}^2}{M_{min}^2} \quad (13)$$

$$B = -2\cdot(1-\frac{1}{X_{max}^2}) - (\frac{R_{e\_max}}{R_{e\_min}})^2(\frac{X_{max}-1/X_{max}}{M_{max}})^2 \quad (14)$$

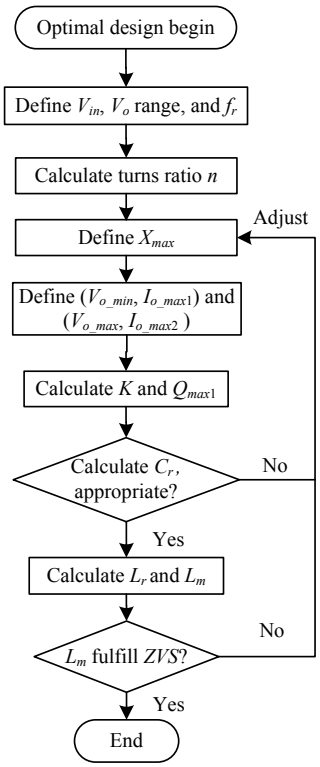

Fig. 6. Flow chart of the resonant tank design.

$$C = -[(1 - \frac{1}{X_{max}^2})^2 + (\frac{R_{e\_max}}{R_{e\_min}})^2 \frac{(X_{max} - 1/X_{max})^2}{M_{max}^2 - 1}] \quad (15)$$

After that, the LLC resonant tank parameters L_r, C_r and L_m can be determined. The following is the step-by-step design procedure, which is illustrated in Fig. 6.

Before it is designed, the initial parameters of the full bridge LLC converter should be defined, such as the current I_{o_max1} = I_{MAX} = 50 A, I_{o_max2} =40 A, the input and output voltage range, the maximum output power and the maximum switching frequency. The input voltage seen by the LLC converter is determined by the front PFC output, whose variation is about ±20 V with a nominal value of 400 V. The output voltage is determined by the battery modules. Here, the charger is designed to charging two kinds of battery systems, 60 V systems with 30 cells and 48 V systems with 24 cells. Then, the output voltage of the charger varies from V_{o_min} = 36 V to V_{o_max} = 72 V, with a nominal value of V_{o_nom} = 58 V at the maximum output power. In this design, f_r = 220 kHz is chosen.

A. Selecting the Transformer Turns Ratio, n

The transformer turns ratio should be selected at the resonant frequency, where the gain is unity. It can be calculated as:

$$n = \frac{V_{in\_norm}}{V_{o\_norm} + V_F} \quad (16)$$

Where, V_F is the diode voltage drop of the output rectifier.

B. Maximum Switching Frequency, X_{max}

The maximum switching frequency of the resonant converter is limited by the control circuit, the driver circuit and the reflected junction capacitance of the output rectifiers. Ref. [16] demonstrates that the normalized dc gain equation of the converter is modified with the rectifier junction capacitances. The circuit resonates with the parasitic capacitances when switching frequency is too high. As a result, the output voltage increases with the switching frequency, which deviates from the original design. Limiting the maximum switching frequency is an approach to prohibit this. In addition, the maximum switching frequency should be limited to $2f_r$ to $2.5f_r$. Here, X_{max} is chosen as:

$$X_{max} = \frac{f_{max}}{f_r} = 2 \quad (17)$$

C. Calculating the Ratio, K

The ratio K of L_m to L_r can be designed with the two charging points (V_{o_min}, I_{o_max1}) and (V_{o_max}, I_{o_max2}) in Fig.3. It can be calculated using (12).

D. Quality Factor Q_{max1} and Characteristic Impedance Z_o

The maximum quality factor Q_{max1} at (V_{o_max}, I_{o_max2}), i.e. (72 V, 40 A), can be calculated using (7). The characteristic impedance Z_o of the resonant tank can be derived from (9) with Q_{max1} and R_{e_max}.

E. Calculating the Resonant Capacitor, C_r

The resonant capacitor value is given by:

$$C_r = \frac{1}{2\pi f_r Q_{max1} R_{e\_max}} \quad (18)$$

If C_r is not an appropriate value for commercial product selection, it can have fine tuning while guaranteeing the two charging points (V_{o_min}, I_{o_max1}) and (V_{o_max}, I_{o_max2}) within the PFM control. Once the value of the resonant capacitor is determined, the resonant inductor value and the transformer magnetizing inductor value can be calculated using (19) and (20).

$$L_r = \frac{1}{4\pi^2 f_r^2 C_r} \quad (19)$$

$$L_m = KL_r \quad (20)$$

F. ZVS Requirements

In order to achieve ZVS at f_{max} with a duty cycle of 0.5, L_m must meet the inequality expressed of (21). If it is not satisfied, the dead time in (21) should be set again or the aforementioned design should be tuned.

$$L_{m\_max} < \frac{nV_{o\_min}t_{dead}}{4f_{max}V_{in\_max}C_{HB}} \quad (21)$$

Here, C_{HB} is the equivalent parasitic capacitor in the middle point of the phase legs Q1 and Q2, and t_{dead} is the dead-time.

III. PRACTICAL DESIGN CONSIDERATIONS

A. MOSFET and Output Diode Selection

When the resonant tank parameters are decided, the minimum switching frequency can be derived by (22) and (23). Then the resonant peak current through the MOSFET can be calculated approximately using (24). In order to decrease the losses, low $R_{DS(ON)}$ MOSFETs should be selected.

$$f_{min} = X_{min} f_r \tag{22}$$

$$X_{min} = \sqrt{\frac{1}{1 + K[1 - 1/M_{\max}^2]}} \tag{23}$$

$$i_{p\_max} = \sqrt{(\frac{\pi f_r I_{o\_nom}}{2nf_{min}})^2 + (\frac{n(V_{o\_max} + V_F)}{4 f_r L_m})^2} \tag{24}$$

The output diode average current can be calculated by (25) with the same average output current.

$$I_D = 0.5 I_{o\_nom} \tag{25}$$

Since the diodes at the secondary side operate with ZCS turn-off, the forward drop V_F and junction capacitance C_j are among the main considering factors in diode selection. The available products include Schottky and Ultrafast diodes. Although Schottky diodes have a lower V_F, they demonstrate a relatively higher C_j when compared with ultrafast diodes. As mentioned in section II, this will limit the maximum switching frequency. Therefore, ultrafast diodes are a better choice.

B. Resonant and Output Capacitors Selection

Assuming the resonant capacitor voltage waveform is sinusoidal, the RMS ac voltage value for the resonant capacitor is given by (26). Then, a Polypropylene film capacitor with a permissible voltage can be selected.

$$V_{c\_rms} = \frac{i_{p\_max}}{2\sqrt{2}\pi f_{min} C_r} \tag{26}$$

A very high ripple current on the secondary side needs to be handled by the output capacitors. This can be calculated approximately using (27). According to this value, the combination of a Polypropylene film capacitor and an Electrolytic capacitor is used.

$$I_{Co} = \sqrt{2I_D^2 - I_{o\_nom}^2} \tag{27}$$

C. Resonant Inductor and Transformer Design

The area product (A_P) denotes the size of the magnetic components and is usually used for design. The A_P of the transformer and inductor can be expressed as:

$$AP_{Lr} = \frac{L_r \Delta i_r I_P}{\Delta B J K_u} \tag{28}$$

$$AP_{Tr} = \frac{L_m \Delta i_m (I_P + I_S / n)}{\Delta B J K_u} \tag{29}$$

Where, I_P and I_S are the primary and secondary RMS currents. Δi_r and Δi_m are the peak-peak currents of the inductor L_r and the transformer magnetizing inductor L_m. ΔB, J and K_u are the flux density, the current density, and the window utility factor, respectively [17]. When magnetic cores are selected, the winding number N_{Lr} of L_r and the secondary winding number N_{Tr_sec} of the transformer T_r can be obtained from:

$$N_{Lr} = \frac{L_r \Delta I_{Lr}}{\Delta B A e_{Lr}} \tag{30}$$

$$N_{Tr\_sec} = \frac{V_{o\_max} + V_F}{2 f_r \Delta B A e_{Tr}} \tag{31}$$

Where, Ae_{Lr} and Ae_{Tr} are the cross section areas of the

TABLE I
DESIGN SPECIFICATIONS AND PARAMETERS

	Parameters	Value
Design Spec.	Input Voltage : V_{in_nom} (V_{in_min}~V_{in_max})	400V ±20 V
	Output Voltage : V_{o_nom} (V_{o_min}~V_{o_max})	58V(36~72V)
	Output Power at 58V : P_{o_nom}	2900 W
	Output Current at 58V : I_{o_nom}	50 A
	Resonant Frequency : f_r	220 kHz
	Maximum Switching Frequency : f_{max}	440 kHz
Design Param.	Ratio of L_m to L_r : K	4.1
	Transformer Ratio : n	14:2:2
	Resonant Inductor : L_r	24 μH
	Resonant Capacitor : C_r	22 nF
	Magnetizing Inductance : L_m	98 μH
	Maximum DC gain : M_{max}	1.25
	Dead Time : t_{dead}	200 ns

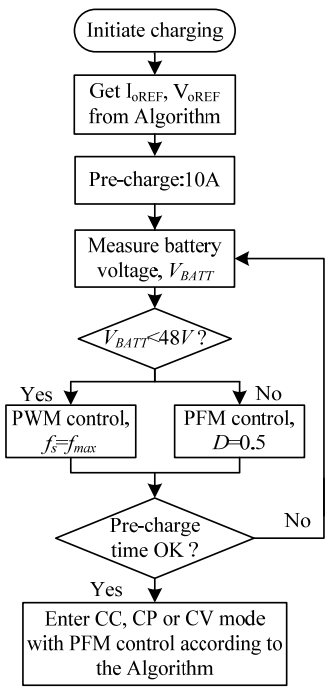

Fig. 7. Simplified flowchart of PFM&PWM combined control at the pre-charge mode.

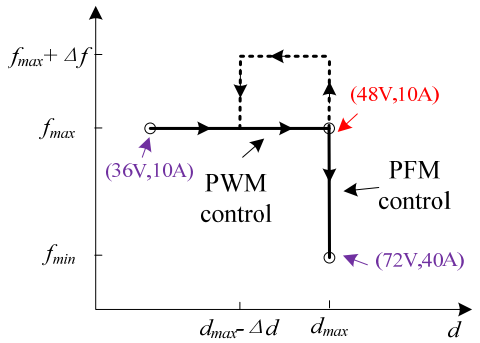

Fig. 8. Diagram of the combined control with hysteresis.

TABLE II
POWER COMPONENT USED IN THE PROTOTYPE CONVERTER

Component	*Manufacturer*	*Part #*
MOSFET	*Infineon*	IPW60R099C6
Diode Rectifiers	*ST*	*STTH6003CW*
Resonant Capacitor	*WIMA*	*MKP10*-22 nF
Resonant Inductor	*TDK*	PQ32/30- PC95
Transformer	*TDK*	2×EE42/42/15-PC95

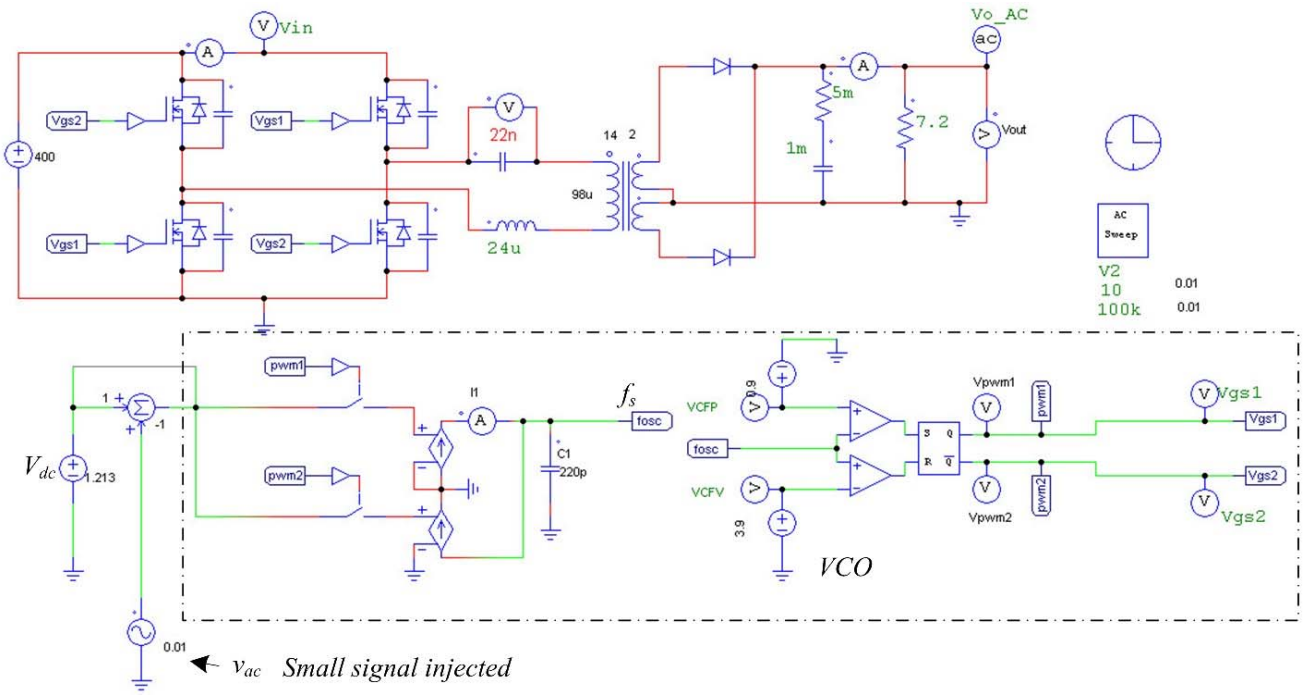

Fig. 9. LLC simultaion model for ac analysis in PSIM.

inductor and transformer cores. Then, the resonant inductor and transformer can be designed.

D. Power Limit Restrictions and Control Design

The V-I plane provided in Fig. 3 illustrates the limitations on the output voltage, output power and output current, which are implemented by software. In order to easily use the PFM&PWM combined control, digital control has been adopted for the charger module. In addition, it can be easily paralleled by the upper controller to charge higher capacity battery packs.

From the analysis above, the converter is designed to work with the PFM control at the two charging points (V_{o_min}, I_{o_max1}) and (V_{o_max}, I_{o_max2}), which indicates that the batteries' CC, CP, and CV charging modes are all within the PFM control range. Then, the boundary of the combined PFM&PWM control happens at the Pre-charge mode, which is just (48 V, 10 A) at f_s=f_{max} with the design parameters in Table I. Fig. 7 is a simplified flowchart of the combined control in the pre-charge mode. At the boundary charging point, the hysteretic type control in Fig. 8 has been adopted to avoid control oscillation.

When designing the controller, an exact expression for the control-to-output transfer function $G_v(s)$ may be necessary. However, modeling the dynamic characteristics of the LLC converter is complex due to its multi resonance [13], [18]. Thanks to powerful simulation tools, they can be easily obtained from simulations, such as PSIM. Fig. 9 shows a LLC simulation model for ac analysis in PSIM. In this figure, V_{dc} and f_s are the input voltage and output frequency of the VCO (voltage controlled oscillation), and v_{ac} is the small signal injected into the system for ac analysis. The conversion ratio f_s/V_{dc} of the VCO is 136.4 kHz/V. Then, the switching frequency f_s is 165.5 kHz at (72 V, 10 A) with V_{dc} =1.213V, while it is 162.3 kHz at (72 V, 40 A) with V_{dc} =1.190V. The dynamic characteristics of the converter at (72 V, 40 A) and (72 V, 10 A) in CV mode are shown in Fig. 10. As in Ref. [13], [18], the two-pole, one-zero voltage feedback $G_c(s)$ in

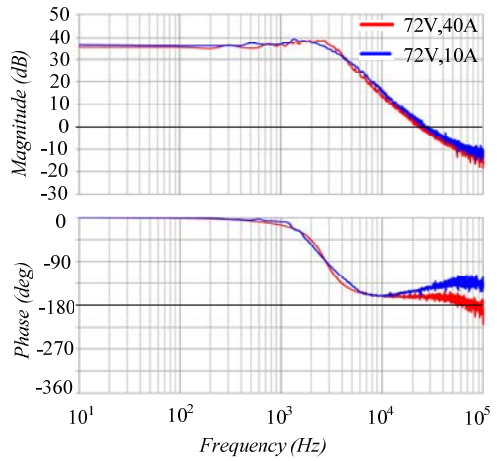

Fig. 10. Control to output transfer function at (72V, 40A), (72V, 10A) in CV charging mode.

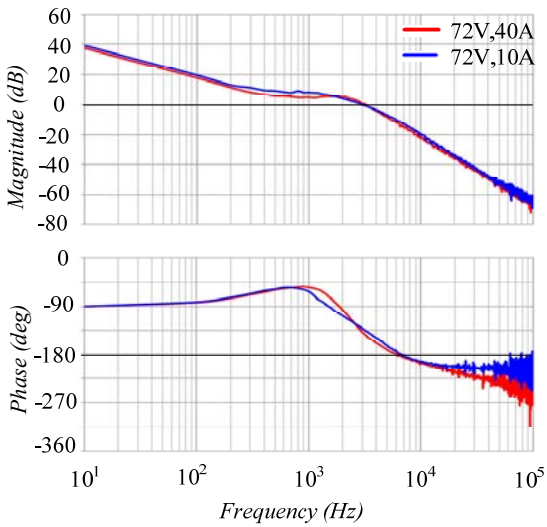

Fig. 11. Loop gain characteristic after compensation at (72V, 40A), (72V, 10A) in CV charging mode.

(32) is used to compensate the loop gain characteristics. When compensated with K_c=71.4, ω_z=3.5×10^3 rad/s, and ω_p=9.9×10^4 rad/s, the loop gain characteristics of the converter are shown in Fig. 11. It has enough stability at the cutoff frequency f = 3 kHz. The dynamic characteristic of the converter at other charging modes can be compensated with a similar procedure.

$$G_c(s) = \frac{K_c(1+\frac{s}{\omega_z})}{s(1+\frac{s}{\omega_p})} \quad (32)$$

IV. Experimental Results

A prototype of the full-bridge LLC resonant converter, as shown in Fig. 12, was built to provide an experimental evaluation of the analytical work presented in this paper. The design criteria for the prototype are provided in Table I.

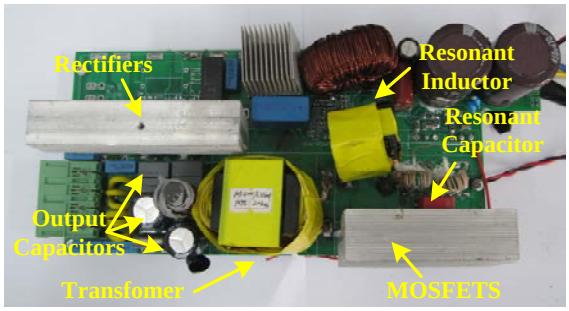

Fig. 12. Experimental prototype.

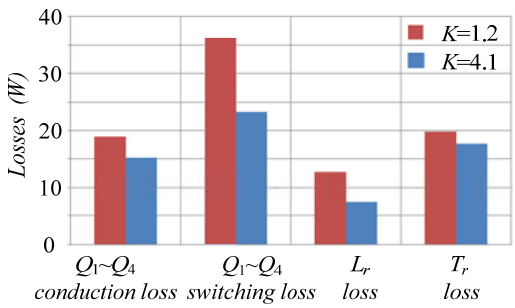

Fig. 13. Calculated losses comparison between the proposed design K=4.1 and the conventional design K=1.2 at 58V/ 2900W output.

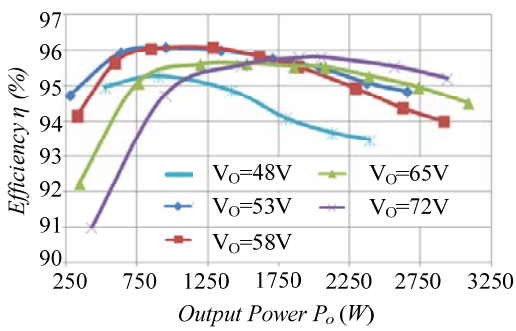

Fig. 14. Measured Efficiency at V_{in}= 400V.

When compared with the conventional design result K=1.2 by Eq. (1), a larger ratio K=4.1, as shown in Table I, has been obtained with the proposed design procedure. Table II gives the key components used in the prototype converter.

Fig. 13 is a calculated loss comparison between the proposed design K=4.1 and the conventional design K=1.2 at a 58 V/2900 W output. This shows that the proposed design can cut down the losses of the primary switches' and magnetic elements, which will improve the converter's efficiency. This comparison has verified the effectiveness of the proposed solution. Efficiency curves of a converter with the proposed method are given in Fig. 14 for output voltages of 48 V, 53 V, 58 V, 65 V and 72 V. A peak efficiency of 96% has been achieved.

Fig. 15 show the experimental waveforms of the Q1 driver voltage (v_{GS1}), voltage across Q1 (v_{DS1}) and resonant tank current (i_r) at V_{in} = 400 V. As shown in Fig. 15(a), the

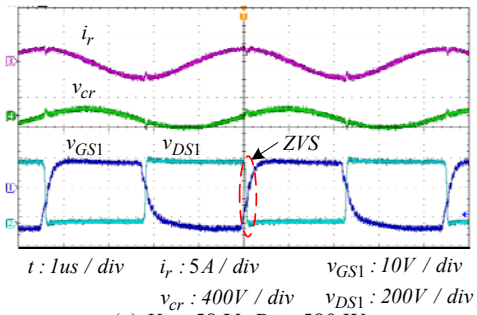

(a) V_o = 58 V, P_o = 580 W.

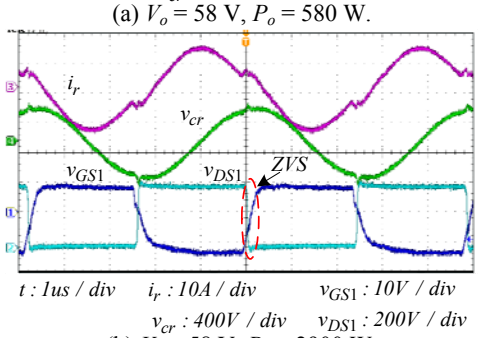

(b) V_o = 58 V, P_o = 2900 W.

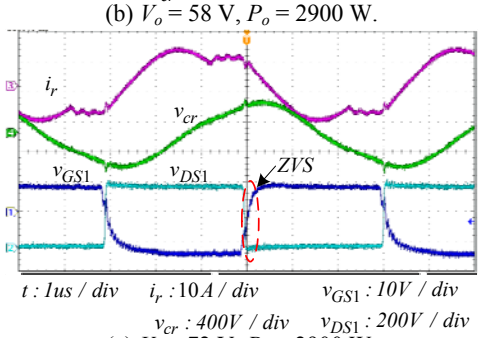

(c) V_o = 72 V, P_o = 2900 W.

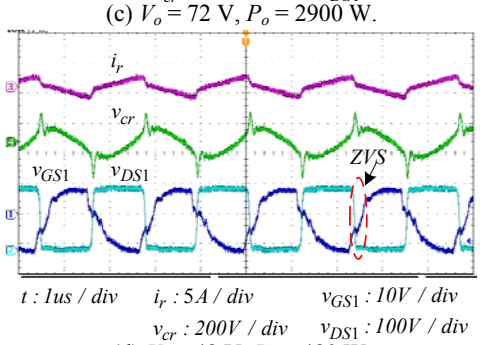

(d) V_o = 48 V, P_o = 480 W.

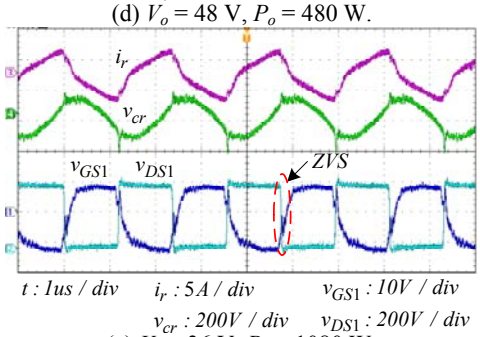

(e) V_o = 36 V, P_o = 1080 W.

Fig. 15. Waveforms of Q1 driver voltage (v_{GS1}), voltage across Q1 (v_{DS1}), and resonant tank current (i_r) at different load ((a) *Vo* = 58 V, *Po* = 580 W; (b) *Vo* = 58 V, *Po* = 2900 W; (c) *Vo* = 72 V, *Po* = 2900 W; (d) *Vo* = 48 V, *Po* = 480 W; (e) *Vo* = 36 V, *Po* = 1080 W).

switching frequency is f_s = 224.4 kHz at V_o = 58 V and P_o = 580 W, which is close to the resonant frequency.

The waveforms in Fig. 15(b) are given at V_o = 58 V and at the maximum output power P_o = 2900 W. Fig. 15(c) presents the waveforms at the maximum output voltage and power, while operating at the minimum frequency. Fig. 15(d) provides the waveforms at V_o = 48 V and P_o = 480 W with f_s = f_{max}, which is the boundary charging point between the PFM control and the PWM control. With the same output voltage above resonant frequency f_r, the switching frequency f_s of the LLC converter decreases with increasing loads. As shown in Fig. 15(e), when the converter runs with f_s = f_{max} at V_{o_min} = 36 V, its output current is 30 A and smaller than I_{o_max1} after fine tuning. Then, it can be inferred that f_s at (V_{o_min}, I_{o_max1}) is smaller than f_{max}, which fulfills the design requirement that the charging point should be within the PFM control range.

In Fig. 15, the primary switches can achieve the ZVS turn-on condition. Since (72 V, 40 A) at f_{min} and (36 V, 30 A) at f_{max} are the worst conditions for the LLC converter's ZVS achievement within the PFM control, the charger can achieve ZVS turn-on during the whole range of the batteries' CC, CP and CV charging modes.

V. CONCLUSION

For battery charging applications, this paper illustrates the resonant tank design considerations of a LLC resonant converter based on FHA analysis. By combining the features of the LLC converter and the characteristics of the battery charging profile, a simple design procedure is proposed to increase the inductance ratio K of L_m to L_r and to improve the efficiency of the charger.

When compared with the ratio of the conventional LLC design K=1.2 at the minimum normalized output voltage gain M_{min} and zero load, the proposed design with two charging points, (V_{o_min}, I_{o_max1}) and (V_{o_max}, I_{o_max2}), can give a much larger ratio, K=4.1. As verified by a calculated losses comparison, the proposed design can cut down the primary conduction and turn-off losses.

A 2.9 kW prototype is built to verify the design. It converts 400 V from the Boost PFC to an output voltage range of 36 V to 72 V dc. Experimental results show that a prototype designed with the proposed method can realize the primary switches' ZVS turn-on during the whole range of the batteries' CC, CP and CV charging modes. In addition, a peak efficiency of 96% can be achieved by the proposed solution.

ACKNOWLEDGMENT

This work was supported by the Natural Science Foundation of Jiangsu, China (BK2012794 BK20140812), the Industry-academic Joint Technological Innovations Fund Project of Jiangsu (BY2014003-12), and Jiangsu province university

outstanding science and technology innovation team project.

REFERENCES

[1] A. Khaligh and S. Dusmez, "Comprehensive topological analysis of conductive and inductive charging solutions for plug-in electric vehicles," *IEEE Trans. Veh. Technol.,* Vol. 61, No. 8, pp.3475-3489, Oct. 2012.

[2] F. Musavi, M. Craciun, D.S. Gautam, W. Eberle, W. G. Dunford, "An LLC resonant DC-DC converter for wide output voltage range battery charging applications," *IEEE Trans. Power Electron.*, Vol. 28, No. 12, pp. 5437-5445, Dec. 2013.

[3] Haoyu Wang, Serkan Dusmez, and Alireza Khaligh. "A novel approach to design EV battery chargers using SEPIC PFC stage and optimal operating point tracking technique for LLC converter," in *Proc. IEEE Appl. Power Electron. Conf. Expo.*, pp. 1683-1689, 2014.

[4] A. K. S. Bhat, "A generalized steady-state analysis of resonant converters using two-port model and Fourier-series approach," *IEEE Trans. Power Electron.*, Vol. 13, No. 1, pp. 142-151, Jan. 1998.

[5] A. J. Forsyth, G. A. Ward, and S. V. Mollov, "Extended fundamental frequency analysis of the LCC resonant converter," *IEEE Trans. Power Electron.*, Vol. 18, No. 6, pp. 1286-1292, Nov. 2003.

[6] N. H. Kutkut, C. Q. Lee, and I. Batarseh, "A generalized program for extracting the control characteristics of resonant converters via the state-plane diagram," *IEEE Trans. Power Electron.*, Vol. 13, No. 1, pp. 58-66, Jan. 1998.

[7] S. S. Hong, S. H. Cho, C. W. Roh, and S. K. Han, "Precise analytical solution for the peak gain of LLC resonant converters," *Journal of Power Electronics*, Vol. 10, No. 6, pp. 680-685, Nov. 2010.

[8] B. Lu, W. Liu, Y. Liang, F. C. Lee, and J. D. van Wyk, "Optimal design methodology for LLC resonant converter," in *Proc. IEEE Appl. Power Electron. Conf. Expo.*, pp. 533-538, 2006.

[9] S. De Simone, C. Adragna, C. Spini, and G. Gattavari. "Design-oriented steady state analysis of LLC resonant converters based on FHA," in *Proc. IEEE Symp. on Power Electron., Elect. Drives, Automation and Motion*, pp. 200-207, 2006.

[10] X. Fang, H. Hu, F. Chen, U. Somani, E. Auadisian, J. Shen, and I. Bataresh, "Efficiency-oriented optimal design of the LLC resonant converter based on peak gain placement," *IEEE Trans. Power Electron.*, Vol. 28, No.5, pp. 2285-2296, May 2013.

[11] H. Pan, C. He, F. Ajmal, H. Chen, and G. Chen, "Pulse-width modulation control strategy for high efficiency LLC resonant converter with light load applications," *IET Power Electron.*, Vol. 7, No. 11, pp. 2887-2894, Aug. 2013.

[12] J. Yamamoto, T. Zaitsu, S. Abe, and T. Ninomiya, "PFM and PWM hybrid controlled LLC converter," *IEEE International Power Electron. Conf.*, pp. 177-182, May 2014.

[13] B. Yang, "Topology investigation for frontend DC/DC power conversion for distributed power systems," Ph. D. dissertation, Virginia Polytechnic Institute and State University, Blacksburg, VA, 2003.

[14] S. Chudjuarjeen, A. Sangswang, and C. Koompai, "An improved LLC resonant inverter for induction-heating applications with asymmetrical control," *IEEE Trans. Ind. Electron.*, Vol. 58, No. 7, pp. 2915-2925, Jul. 2011.

[15] J. K. Jeong, B. M. Han, J. Y. Lee, and N. S. Choi, "High-efficiency grid-tied power conditioning system for fuel cell power generation," *Journal of Power Electronics*, Vol. 11, No. 4, pp. 551-560, Jul. 2011.

[16] B.-H. Lee, M.-Y. Kim, C.-E. Kim, K.-B. Park, and G.-W. Moon, "Analysis of LLC resonant converter considering effects of parasitic components," in *Proc. IEEE Telecommun. Energy Conf.*, pp. 1–6, 2009.

[17] B.-C. Kim, K.-B. Park, and G.-W. Moon, "Asymmetric PWM control scheme during hold-up time for LLC resonant converter," *IEEE Trans. Power Electron.*, Vol. 59, No. 7, pp. 2992-2997, Jul. 2012.

[18] C. H. Park, S. H. Cho, J. Jang, S. K. Pidaparthy, T. Ahn, and B. Choi, "Average current mode control for LLC series resonant DC-to-DC converters," *Journal of Power Electronics*, Vol. 14, No. 1, pp. 40-47, Jan. 2014.

Wenjin Sun was born in Jiangsu Province, China, in 1988. He received his B.S. degree in Electrical Engineering from the Nanjing University of Aeronautics and Astronautics (NUAA), Nanjing, China, in 2011. He is presently working toward his Ph.D. degree in Electrical Engineering at NUAA. His current research interests include topologies and control methods for power converters, distributed power generation and spacecraft power systems.

Hongfei Wu was born in Hebei Province, China, in 1985. He received his B.S. and Ph.D. degrees in Electrical Engineering and Power Electronics and Power Drives from the Nanjing University of Aeronautics and Astronautics (NUAA), Nanjing, China, in 2008 and 2013, respectively. From June 2012 to July 2012, he was a guest Ph.D. student at the Institute of Energy Technology, Aalborg University, Aalborg, Denmark. Since 2013, he has been with the Faculty of Electrical Engineering, NUAA. He is presently a Lecturer in the College of Automation Engineering, NUAA. He has authored or co-authored more than 90 peer-reviewed papers published in journals and conference proceedings. He is the holder of more than 17 patents. His current research interests include power converters, distributed power generation and spacecraft power systems. Dr. Wu was awarded as an Outstanding Reviewer of the IEEE Transactions on Power Electronics (2013).

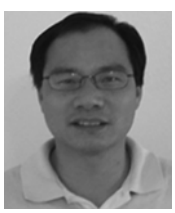

Haibing Hu received his B.S. degree from the Hunan University of Technology, Hunan, China, in 1995, and his M.S. and Ph.D. degrees in Electrical Engineering from Zhejiang University, Zhejiang, China, in 2003 and 2007, respectively. Since 2007, he has been with the Faculty of Electrical Engineering, Nanjing University of Aeronautics and Astronautics (NUAA), Nanjing, China. He is presently a Professor in the College of Automation Engineering, NUAA. From 2009 to 2012, he was a Postdoctoral Research Fellow in the Department of Electrical Engineering, University of Central Florida, Orlando, FL, USA. He is the author or coauthor of more than 70 technical papers published in journals and conference proceedings. His current research interests include digital control in power electronics, multilevel inverters, digital control system integration for power electronics, and applying power electronics to distributed energy systems and power quality.

Yan Xing was born in Shandong Province, China, in 1964. She received her B.S. and M.S. degrees in Automation and Electrical Engineering from Tsinghua University, Beijing, China, in 1985 and 1988, respectively, and her Ph.D. degree in Electrical Engineering from Nanjing University of Aeronautics and Astronautics (NUAA), Nanjing, China, in 2000. Since 1988, she has been with the Faculty of Electrical Engineering, NUAA, and is presently a Professor in the College of Automation Engineering, NUAA. She has authored more than 100 technical papers published in journals and conference proceedings. She has also published three books. Her current research interests include topologies and control methods for dc-dc and dc-ac converters.